Received: 28 June 2022 | Revised: 22 August 2022 | Accepted: 25 August 2022

DOI: 10.1002/bip.23525

ARTICLE

Biopolymers WILEY

Energetically unfavorable protein angles: Exploration of a conserved dihedral angle in triosephosphate isomerase

Patrick W. Allen | Jordan A. Cook | Anh N. Colquhoun | Eric J. Sorin | Enrico Tapavicza | Jason P. Schwans

Department of Chemistry and Biochemistry, California State University Long Beach, Long Beach, California, USA

Correspondence
Jason P. Schwans, Department of Chemistry and Biochemistry, California State University Long Beach, Long Beach, CA 90840, USA.
Email: jason.schwans@csulb.edu

Funding information
National Institutes of Health, Grant/Award Numbers: R25GM071638, RL5GM118978, TL4GM118980, UL1GM11897; National Institute of General Medical Sciences

Abstract

Over the past 3.5 billion years of evolution, enzymes have adopted a myriad of conformations to suit life on earth. However, torsional angles of proteins have settled into limited zones of energetically favorable dihedrals observed in Ramachandran plots. Areas outside said zones are believed to be disallowed to all amino acids, except glycine, due to steric hindrance. Triosephosphate isomerase (TIM), a homodimer with a catalytic rate approaching the diffusion limit, contains an active site lysine residue (K13) with dihedrals within the fourth quadrant ($\Phi = +51/\Psi = -143$). Both the amino acid and the dihedral angles are conserved across all species of TIM and known crystal structures regardless of ligand. Only crystal structures of the engineered monomeric version (1MSS) show accepted β-sheet dihedral values of $\Phi =$ -135/$\Psi = +170$ but experiments show a 1000-fold loss in activity. Based on these results, we hypothesized that adopting the unfavorable torsion angle for K13 contributes to catalysis. Using both, computational and experimental approaches, four residues that interact with K13 (N11, M14, E97, and Q64) were mutated to alanine. In silico molecular dynamics (MD) simulations were performed using 2JK2 unliganded human TIM as a starting structure. Ramachandran plots, containing K13 dihedral values reveal full or partial loss of disallowed zone angles. N11A showed no detectable catalytic activity and lost the unfavorable K13 dihedral angles across four separate force fields during simulation while all other mutants plus wild type retained activity and retained the conserved K13 dihedral angles.

KEYWORDS
dihedral angles, disallowed, molecular dynamics, mutation, protein design, triosephosphate isomerase

1 | INTRODUCTION

Triosephosphate isomerase (TIM) has been a model enzyme for the study of structure function relationships in proteins, garnering over 199 crystal structures across 42 species.[1] The TIM-barrel quaternary structure is shared by 10% of all known enzymes,[2] making it an attractive system to investigate enzyme design. The enzyme is a homodimer and one monomer of this dimer contains 250 residues, almost 18% of which are highly to completely conserved non-glycine residues.[1] There are three residues, K13, H95, and E167, that are directly involved in contacting the substrate for the interconversion of glyceraldehyde 3-phosphate and dihydroxyacetone phosphate (for simplicity, numbering of residues according to the human form of TIM are used throughout).

It has been observed that some peripheral residues work together as a unit to support enzymatic function as I170 and L230 work together to enhance catalytic E167's as a general base,[3] and thus should be studied in the structural context of the enzyme. One such

feature of TIM are completely conserved dihedral angles for catalytic K13 ($\Phi = +51/\Psi = -143$), which is a conformation of the Ramachandran plot typically adopted by glycine.[4,5] This K13 adopts a type IV β-turn in a "WKMN" sequence without the aid of a surrounding glycine or proline. This relatively unfavorable conformation may have a structural and/or functional purpose. Assuming the side chain is rigid within the active site, were the K13 to adopt a more favorable α-helical or β-sheet conformation then the side chain would be directed toward H95 and away from the substrates' phosphate group. If a loss of this disallowed angle causes mispositioning, then it is expected that a loss in catalytic activity would occur. Understanding the elements of these conserved dihedral features would be an important step that follows identifying residues involved in bond making/breaking, beyond identifying the need for a general base or acid.

Sequence-to-structure prediction programs such as AlphaFold are becoming more accurate with each CASP (critical assessment of protein structure prediction) competition.[6] Given their utility, these programs will likely play increasingly important roles in protein design as they can be used to predict or orient active site residues in theozymes. Historically, these approaches employ template-based strategies, which are informed by structures published on the protein data bank, or a combination of template and template-free methods.[6,7] However, rare but potentially useful features such as TIM's energetically unfavorable angle may be ignored due to a statistically low number of structures employing them. Lakshmi et al. found only 221 disallowed dihedral angles across the protein data bank in 2014 and concluded that these angles played a biologically significant role 50% of the time when conserved.[1] Here, we test this hypothesis using K13 in human TIM (hTIM).

The wild-type (WT) hTIM enzyme was selected for its high resolution crystallography structures (PDB: 2JK2). Four residues in hTIM were selected as candidates for mutation to alanine (N11, M14, Q64, and E97), as the four residues are highly conserved and proximal to the lysine residue. N11 and Q64 are situated near K13's peptide backbone, while M14 is an adjacent residue, and E97 is near the epsilon ammonium group of the lysine residue. W12 or occasionally F12, another functionally conserved TIM residue was not selected due to Tryptophan's role in protein stability.[8,9] While activity and stability can be measured by traditional spectroscopic methods, observation of the K13 dihedral angles conformation cannot. Molecular dynamics (MD) studies were employed to measure K13's preferred conformation upon reaching equilibrium. Due to force field bias toward certain dihedral conformations during protein folding experiments,[10] four separate force fields were employed in this study: AMBER03,[11] AMBER14sb,[12] OPLS-AA,[13] and CHARMM27 + correction mapp CMAP.[14]

2 | METHODS

2.1 | Reagents

All reagents purchased were of the highest purity commercially available. FPLC purification was performed using a Bio-Rad DuoFlow Chromatography system and HisTrap HP and HiDesalting columns (GE Healthcare). Spectroscopy measurements were performed using a Perkin Elmer Lambda 25 spectrophotometer, a PerkinElmer LS-55 fluorescence spectrometer, and a Jasco J-810 spectrophotometer. Cuvettes were from Starna Cells.

2.2 | Purification of his-tagged TIM

The plasmid for the WT hTIM was purchased from Addgene (#50723). The plasmids for hTIM mutants were produced using QuikChange site directed mutagenesis and X10-Gold ultracompetent cells (Agilent Technologies) by introducing the mutations in top EPTIM7 genes encoded on pET3a plasmids. The constructs were expressed and purified based on the protocols described by Borchert et al.[9] and Zhai et al.[15] Protein concentrations were determined according to the method of Gill and Hippel and extinction coefficients calculated using ProtPram on the ExPASy server.[16–18]

hTIM was expressed in *E. coli* BL21 (DE3) cells. Enzyme purification was based on metal-ion and ion-exchange chromatography.[15,17] In this study, the ion-exchange chromatography was omitted, with the same levels of activity for WT enzyme purified using either protocol. Cells were lysed by sonication and the supernatant was collected by centrifugation. The supernatant was loaded on a Ni-NTA column, the column was washed with 200 mM NaCl in 20 mM Tris–HCl, pH 8.0, and the enzyme was eluted using a gradient of 0–250 mM imidazole in 200 mM NaCl, 20 mM Tris–HCl, pH 8.0. Fractions containing the enzyme were pooled and desalted using 5 ml desalting column in 20 mM Tris–HCl, 20 mM NaCl buffer, pH 8.0. Glycerol was added to desalted samples to the final concentration of 20% and aliquots were stored at −80°C.

2.3 | Enzyme assays

Enzyme activity assays were performed at 25°C in 30 mM triethanolamine (TEA) pH 7.6, 1 mM EDTA, 4 mM sodium arsenate, and 1 mM NAD^+. TIM activity was monitored by coupling the assay with the final concentration of 0.04 mg/mL glyceraldehyde-3-phosphate dehydrogenase (GAPDH) and monitoring the formation of NADH (the final concentration of 40 mg/mL) at 340 nm.[15,17,19] Dihydroxyacetone phosphate (DHAP) was used as the substrate in varying concentrations and the activity assays were initiated by the addition of enzyme at the final concentration of 10 nM. Initial rates were calculated and fit to the Michaelis–Menten equation. Activity assays were recorded and averaged from a minimum of three independently prepared samples. Previous studies have reported a low level of background isomerization likely from contaminating TIM in the commercially available GAPDH.[20,21] A similarly low level of background isomerization was observed in this study.

2.4 | Circular dichroism

Enzyme solutions for circular dichroism (CD) were buffer exchanged (3 × 400 μl) in 10 mM sodium phosphate, pH 7.5 and then diluted with 10 mM sodium phosphate, pH 7.5 to the final enzyme concentration of 150 mg/ml.[8] A cuvette with a 0.1 cm path length was

loaded with 220 μl of protein solution and ellipticity was measured with far-UV scans from 185 to 260 nm. Four scans were recorded and averaged for each sample. Reference samples without protein were recorded and subtracted from each spectrum.

Ellipticities are reported as the molar ellipticity. The alpha helical content determined from the CD spectra were calculated using DichroWeb and the CDSSTR, SELCON3, CONTIN, and K2D programs.[22,23] Reference set 3 was used for calculations with CDSSTR, SELCON3, and CONTIN (K2D calculations do not require a reference set). Similar results were obtained for calculations using reference set 6. Spectra were recorded and averaged from a minimum of four independently prepared samples.

2.5 | Fluorescence measurements

Fluorescence spectra were recorded in 20 mM triethanolamine pH 7.4, 1 mM EDTA, 1 mM DTT and 50 mg/mL enzyme at 25°C.[8] The excitation wavelength was 295 nm and emission from 310 to 400 nm was recorded. Background spectra were recorded and subtracted from all experimental measurements. Values and standard deviations reported are from a minimum of three independent experiments. The spectral center of mass (SCM) was calculated using the following equation where I(λ) is the fluorescence intensity at wavelength (I):

$$\mathrm{SCM} = \frac{\Sigma \lambda \mathrm{I}\lambda}{\Sigma \mathrm{I}\lambda}$$

2.6 | Molecular dynamics

Starting structure 2JK2 (hTIM) residues were mutated using SwissProt DeepView.[24] Each mutant was simulated with TIP3P water molecules using OPLS-AA, AMBER03, AMBER14sb, and CHARMM27 + CMAP correction force fields separately for each mutant using GROMACS 2018.4.[25–27] Each structure was energy minimized for 50,000 steps of steepest descent and then equilibrated in an NVT ensemble for 100 ps, NPT ensemble for 100 ps, and then allowed to continue simulating for a 200 ns using V-rescale modified Berendsen Thermostat[28] and a Parrinello-Rahman Barostat[29] at 300 K and 1 atm, respectively. MATLAB was used to generate heatmaps summarizing the results.[30] The final 100 ns of each simulation only was used for analysis. All root-mean-square deviations (RMSD) were computed from MD simulations against the whole protein.

3 | RESULTS AND DISCUSSION

3.1 | Activity assays to evaluate effects of peripheral residue mutation in hTIM

The conversion of DHAP to GAP was first measured for WT and the mutants, due to the ease in obtaining DHAP. Experiments to determine k_{cat}, K_m, and k_{cat}/K_m were conducted using the same approach for N11A, M14A, Q64A, and E97A mutants (Table 1). To minimize contamination of mutants with WT enzyme, separate nickel-affinity columns were used for each mutant in purification via affinity chromatography. WT activity was in agreement with literature values.[17] All mutants, other than N11A showed measurable activity. Previous studies investigating K13 mutations that led to large rate effects ($\sim 10^4$) reported a low level of isomerization in the absence of added TIM.[20,21] The isomerization was suggested to arise from TIM contamination in the commercially available GAPDH used in the assays. A similarly low level of background isomerization was observed in this study. Comparing the velocity for the background isomerization to the enzymatic reactions suggested that a rate effect of $\sim 10^4$ could be observed above the background. This suggests an upper limit of an activity $\sim 10^4$-fold lower than WT for the N11A mutation.

For mutants with measurable activity, all showed a less than a two-fold increase in K_m relative to WT hTIM. The M14A and E97A mutants led to a ~5-fold decrease in k_{cat}/K_m, while the Q64A mutant showed a 16-fold decrease in activity. As noted in the introduction, M14 is an adjacent residue, and E97 is situated near the epsilon ammonium group of lysine. The N11 and Q64 sidechains are situated near the peptide backbone and positioned to interact via hydrogen bonds with the backbone of K13. The different locations of the groups relative to the lysine residue offers a simple structural model for the different rate effects. The M14 side chain points away from K13 but was tested by mutation due to being adjacent to K13 in the primary sequence. Due to the position of the M14 sidechain, mutation to alanine is not predicted to disrupt the K13 sidechain, and little change in activity was observed for the mutant relative to WT. The E97 mutation could perturb hydrogen bonding and/or Van der Waals interactions with the K13 ammonium group, but the multiple degrees of freedom of the lysine sidechain likely limit the ability of the distal groups from stabilizing the unfavorable backbone conformation. Mutation of N11 or Q64, however, residues directly interacting with the K13 backbone, might disrupt the energetically unfavorable K13 backbone conformation and lead to larger rate effects.

While the N11A mutation showed the largest rate decrease, the catalytic role of this residue is not well understood.[31,32] As the N11 sidechain is situated within 3 Å of the K13 backbone amide, one model is that the residue helps stabilize the unfavorable lysine backbone conformation and this conformation helps position the lysine residue (Figure S1a). Analysis of the yeast TIM crystal structure in complex with substrate DHAP bound (1NEY) shows the K13 dihedral angle remaining in the fourth quadrant of the Ramachandran plot ($\Phi = +59/\Psi = -148$), suggesting that the dihedral angle is maintained in the presence of ligand (Figure S1b).[33] In addition, the yeast structure with substrate bound shows the cationic lysine sidechain on the surface of the protein and near both the anionic phosphodianion the carbonyl groups of the bound substrate (Figure S1b).[20,21,33] As noted above, Richard et al. reported that the K13G mutation (mutation of a residue important for phosphate binding) led to a 12,000-fold decrease in k_{cat}, indicating that disruption of phosphate binding substantially affects enzyme activity.[20,21] It is possible that activity is decreased for N11A due to a change in the backbone angles affecting

TABLE 1 Michaelis–Menten kinetics, circular dichroism, and fluorescence results for hTIM enzymes investigated

Enzyme	k_{cat} (s^{-1})	K_m (mM)	k_{cat}/K_m (M^{-1} s^{-1})	%-helical content	SCM
Wild type	$5.3 * 10^2 \pm 42$	0.8 ± 0.2	$6.4 * 10^5 \pm 1.4 * 10^5$	34.9 ± 4.3	347.1 ± 0.2
N11A	No detectable activity[a]	No detectable activity[a]	No detectable activity[a]	30.7 ± 3.8	347.4 ± 0.7
Q64A	$4.5 * 10 \pm 7.6$	1.4 ± 0.3	$4.7 * 10^4 \pm 2.4 * 10^4$	40.7 ± 1.8	348.1 ± 0.4
M14A	$1.4 * 10^2 \pm 51$	1.5 ± 0.3	$1.1 * 10^5 \pm 6.2 * 10^4$	38.3 ± 4.0	345.0 ± 0.2
E97A	$1.9 * 10^2 \pm 16$	1.5 ± 0.3	$1.3 * 10^5 \pm 0.4 * 10^5$	28.8 ± 0.1	349.1 ± 0.2

[a]A low amount of background isomerization limited detection of activity below the background level.

the positioning of the lysine chain and the distance between the K13 sidechain and the substrate phosphodianion.[20,21] Finally, the previous computational and structural studies have also suggested a role for the N11 residue in the TIM reaction mechanism.[31,34,35] A crystal structure of *Leishmania* TIM complexed with a substrate analog showed the N11 sidechain within hydrogen-bonding distance of the O1 oxygen of the substrate analog,[31] and the structure of yeast TIM complexed with DHAP shows an interaction between the N11 side chain and the C-1 OH of the substrate. It is possible that this interaction stabilizes the transition state for deprotonation to form the enediolate intermediate.[20,21] Although this study highlights the importance of N11 in the TIM-catalyzed reaction, additional studies beyond the scope of this investigation will be needed to further dissect the contributions of N11 to catalysis.

3.2 | Effects of enzyme structure evaluated by circular dichroism and fluorescence assays

While the activity experiments were the central experimental measure of the mutational effects, circular dichroism and fluorescence assays were conducted to evaluate if structural perturbations were detected between WT and N11A and when compared to other mutations tested. For the CD data sets a *p*-value of 0.165 ($n = 4$) was found between both WT and N11A data sets in an equal variance 2 sample t-test. The CD data sets show *p*-values for M14A, Q64A, and E97A respectively as; 0.326 ($n = 4$), 0.261 ($n = 4$), and 0.032 ($n = 4$). Similarly, the same equal variance test for the spectral center of mass found a *p*-value of 0.125 ($n = 10$) for N11A and 0.002 ($n = 4$), 0.032 ($n = 4$), and 0.012 ($n = 4$) for M14A, Q64A, and E97A, respectively. A *p*-value greater than 0.05 shows that there is no reason to believe the "centers" of these data sets are statistically different from one another, meaning there is no statistical significance between WT and N11A mutant alpha helical percentage evaluated circular dichroism nor fluorescence measurements. Combined, the CD (Figure S2) and SCM results indicate that the N11A mutation does not perturb the general structure compared to the WT. In contrast, the CD and SCM results both indicate that the E97A mutation does perturb the general structure compared to the WT. For the M14A and Q64A mutants, the CD data indicate that the alpha helical content is not statistically different than WT for either mutant, but the SCM data suggest that the general structure is perturbed by their respective mutations compared to the WT. Overall, the CD and fluorescence results suggested that the larger rate effect for the N11A mutation was not from a substantial perturbation of the secondary or tertiary structure compared to the WT and other mutants tested.

3.3 | Occupancy of K13 dihedrals in hTIM mutants evaluated using molecular dynamics

While x-ray structures are a foundation within protein science, they are still static images of biological enzymes. In contrast, MD can evaluate motion. If the K13 dihedral angles are conserved across published crystal structures, then the question remains: How would they behave if given motion in a MD simulation? The WT protein was simulated to as a reference for mutants of peripheral residues (Figure 2) and to determine if this dihedral conformation continues to be observed while in motion. Four different force fields incorporated into GROMACS were chosen to assess dihedral bias in sampling K13 occupancy: OPLS-AA, AMBER03, AMBER14sb, and CHARMM27. The AMBER14sb forcefield is the most recent AMBER forcefield optimized for three-point water molecules, while AMBER03 has been more extensively used as an older force field. Both AMBER force fields were incorporated into this study to ask if there is consensus between older and newer forcefields. While OPLS-AA was derived from AMBER force field parameters, the CHARMM family of force fields were independently developed. For all four force fields, hTIM retained its original dihedral values within the fourth quadrant.

In contrast to the WT protein, the N11A mutation did not retain the K13 dihedrals within the fourth quadrant, losing this conformation completely during equilibration. While there is no agreement between force fields if the β-sheet or α-helix conformations are preferred instead, it is the only single mutant in this study to adopt alternative conformations. Consequently, it is the only mutant to not show detectable activity. The M14A and E97A mutants retained their energetically unfavorable angles (Figure S3) across the chosen force fields. The Q64A mutant also showed retention of the energetically unfavorable angle in three of the four force fields tested. While the AMBER03 force field shows that Q64A lost the quadrant IV dihedral angles, in contrast to N11A, the lack of agreement between force fields suggests that bias in an individual force field may affect the

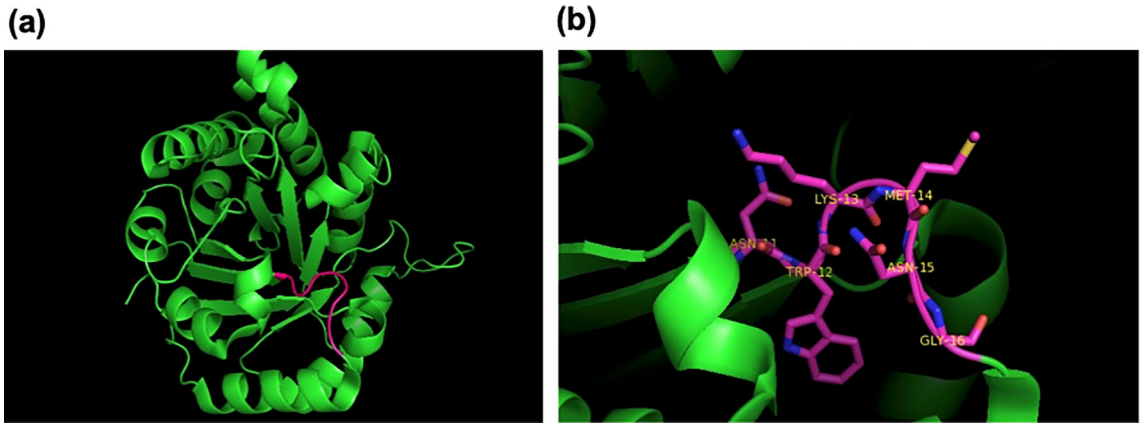

FIGURE 1 (a) Residues 11–16 (magenta) form the type IV beta-sheet turn in 2JK2 hTIM with K13. (b) Loop 1 (magenta) in the greater context of the TIM monomer

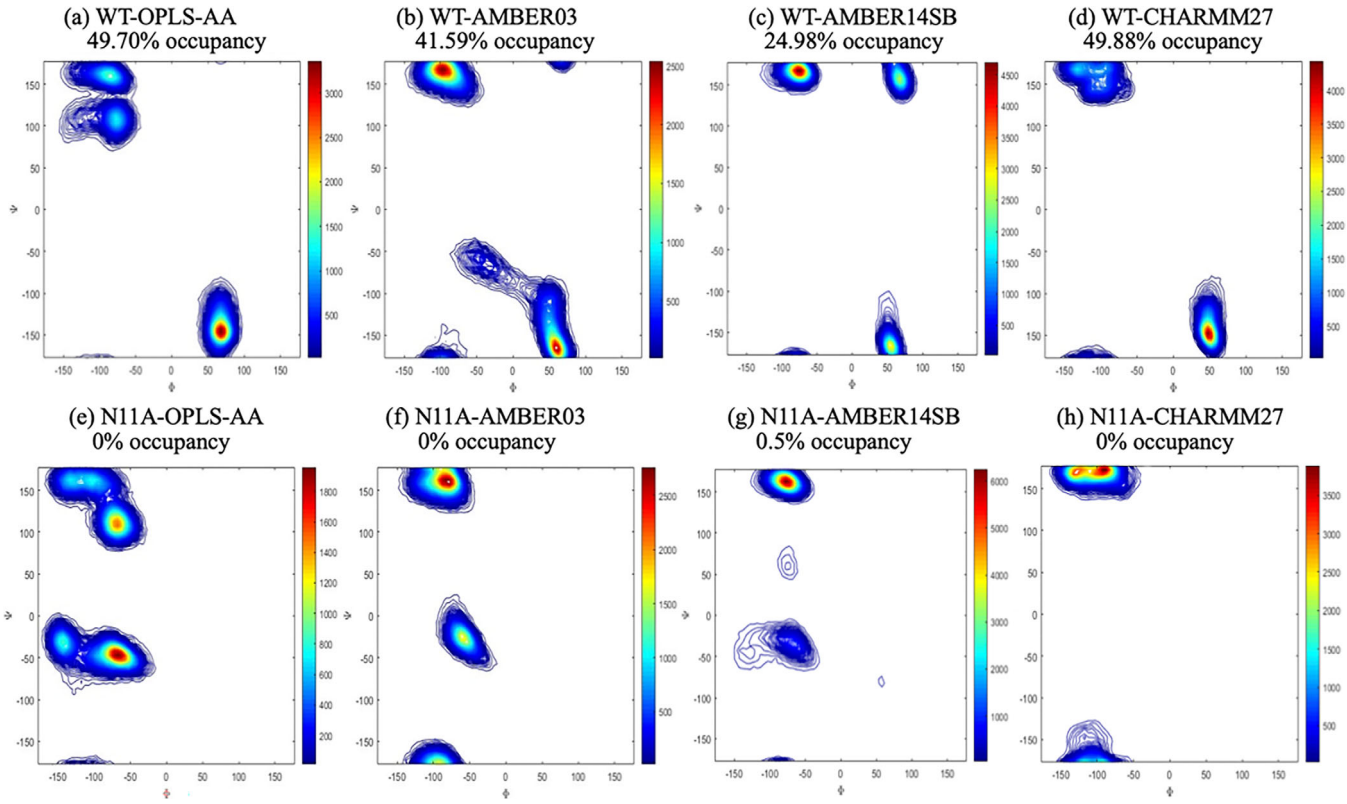

FIGURE 2 Heatmaps of lysine 13 dihedral angles for WT (a–d) and N11A (e–h) over the final 100 ns of molecular dynamics simulations with their respective K13 dihedral angle's percent occupancy of quadrant IV Ramanchandran configuration. Each graph represents 200,000 plotted structures plotted in MATLAB.[30] The color code indicates the number of structures observed within 5° x 5° sized bins

results. However, the agreement among all force fields tested for the N11A mutation suggests dihedral bias inherent in each force field does not contribute to the results and that the dihedral angles in the fourth quadrant are lost in the N11A mutant. Overall, the MD results support the model that N11 is involved stabilizing the energetically unfavorable K13 dihedral angles.

3.4 | Effects of mutations on loop one flexibility evaluated by molecular dynamics

Loop 1 (Figure 1b) contains residues 11–16 in human TIM. There is potential for mutation of peripheral residues to destabilize loop 1 out of type IV β-turn, and thus affect the shape of TIM active site. For the

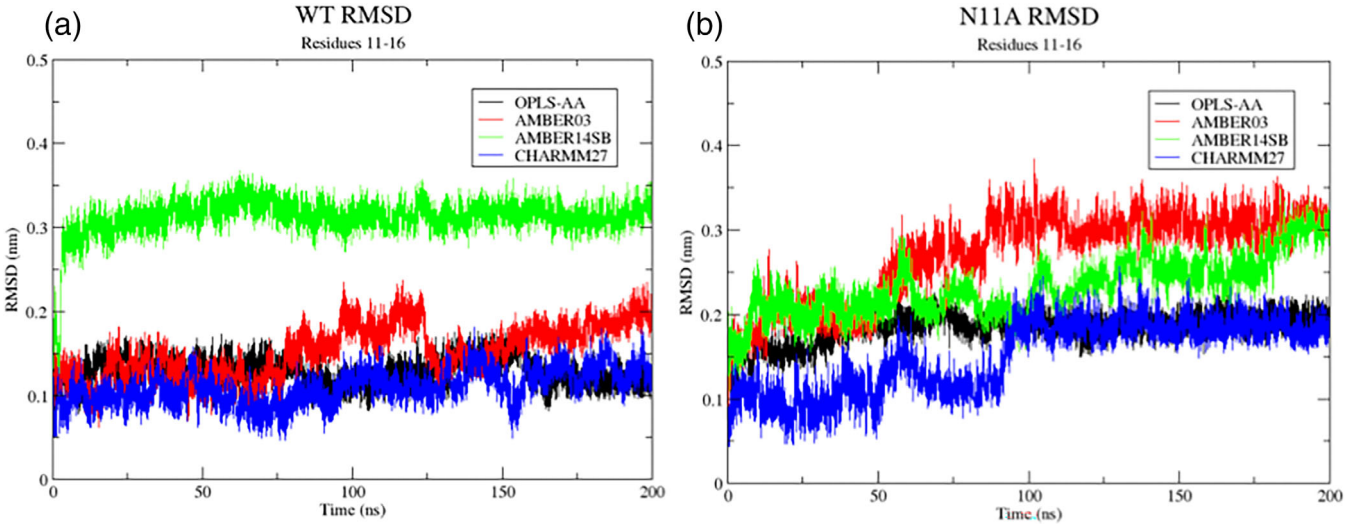

FIGURE 3 Root mean-square deviation of loop 1 (residues 11–16) against whole protein for WT (a) and N11A (b) TIM. Black-colored RMSD corresponds to the OPLS-AA force field, red-colored RMSD to AMBER03, green-colored RMSD to AMBER14SB, and blue-colored RMSD to CHARMM27

OPLS-AA and CHARMM27 force fields, the N11A mutation did not show increased RMSD compared to the WT for all four force fields. While the Amber03 force field showed an approximate 2 Å increase in RMSD for N11A, interpretations will only be made when all four force fields agree. There is no consensus suggesting that the mutation destabilizes the local loop 1 structure by MD (Figure 3). Neither M14A, Q64A, nor E97A loop 1 show increased deviation compared to WT (Figure S4). Overall RMSD results indicate that the local structure of loop 1 is relatively rigid despite lacking the secondary structure, and that mutations of peripheral residues, including residues within loop 1 do not significantly decrease rigidity.

Although the flexibility between mutant and WT profiles are similar for loop 1, that does not mean that the potential states of this loop are the same between TIM structures. Both AMBER03 and CHARMM27 force fields sampled a potentially different state in loop 1 for the N11A mutant after 100 ns (Figure 3). Further MD experiments on other N11 mutants would provide greater context for explaining the shift in loop 1 RMSD, but for now the shift is noted for the future work.

4 | CONCLUSION

The WT, M14A, and E97A all retained the conserved K13 dihedral angles and had observable activity. The Q64A mutation showed a modest rate decrease and the K13 dihedral angles were retained in three of the four force fields tested. A future direction will be to further dissect the potential role of Q64 in stabilizing the K13 dihedral angles and investigating potential biases that may lead to different results using different force fields. In contrast, the N11A mutation had the largest effect on both the K13 dihedral angles and activity. While the mutation's activity could have been the result of a misfolded enzyme, the combination of circular dichroism, intrinsic tryptophan fluorescence, and RMSD measurement by MD show that it is less likely that the N11A mutation overall structurally deviates from the wild type. The M14A, Q64A, and E97A mutants exhibited structural perturbations when observed by CD, SCM, or both spectral methods but still retained observable activity. A longer term goal of this type of study is to build on the results presented herein with more extensive high-resolution structural analysis. It is anticipated that the detailed structural analysis may increase our understanding of the sensitivity of enzymatic activity to local changes in structure, and this may help in designing specific interactions and/or avoiding interactions.

It should be noted that the K13 dihedral angle conservation is not restricted to lysine: A K13M mutant (PDBID: 4ZVJ) in hTIM maintains the ($\Phi = +69/\Psi = -139$) dihedral angles, making it unlikely that the lysine side chain contacts aid in stabilization. MD simulations demonstrate the loss of the unfavorable K13 dihedral angles in the N11A mutant. Together with the loss of activity in N11A, this indicates a potential link between catalysis and the conserved dihedral conformation, as suggested by findings of Lakshmi et al.[1] Connecting activity effects to the dihedral angles is challenging, but the combination of experimental and computational results helps provide information in this complicated structural context.

However, it could be that N11 is strictly needed for binding the substrate phosphate group in order for loop 6 to close around the substrate or involved with stabilizing the intermediate. Indeed, the location of N11 near the K13 backbone and near the substrate suggest multiple potential roles for this residue in catalysis. Binding studies with intermediate analog 2-phosphoglyceric acid (2PG) and suicide inhibitor bromohydroxyacetone phosphate (BHAP)[36] would provide additional clarity on this possibility. Additional mutations to N11 such as N11Q, N11L, and N11H may better define N11's role as necessary for substrate binding versus being necessary for K13 stabilization.

Triosephosphate isomerase is positioned to continue the conversation on catalytically relevant residues with conserved quadrant IV dihedral angles. Should the link between dihedral angles and catalytic activity be firmly established, then that would be the first step in exploring unfavorable dihedral angles for the enhancement of theozymes.

ACKNOWLEDGMENTS

Research reported in this publication was supported by the National Institute of General Medical Sciences of the National Institutes of Health under award number R25GM071638, BUILD Small Equipment and Computers Grant UL1GM11897, TL4GM118980, and RL5GM118978, and the Carl E. Riley Endowed STEM Award. The authors thank Justin Lemkul for their well-designed GROMACS tutorials.

FUNDING INFORMATION

Research reported in this publication was supported by the National Institute of General Medical Sciences of the National Institutes of Health under award number R25GM071638, BUILD Small Equipment and Computers Grant UL1GM11897, TL4GM118980, and RL5GM118978, and the Carl E. Riley Endowed STEM Award.

CONFLICT OF INTEREST

The authors claim no conflict of interest.

DATA AVAILABILITY STATEMENT

The data that support the findings of this study are available from the corresponding author upon reasonable request.

ORCID

Patrick W. Allen https://orcid.org/0000-0002-8400-5823
Jordan A. Cook https://orcid.org/0000-0001-8979-6882
Eric J. Sorin https://orcid.org/0000-0003-4081-1142
Enrico Tapavicza https://orcid.org/0000-0002-0640-0297
Jason P. Schwans https://orcid.org/0000-0001-8011-3758

REFERENCES

[1] B. Lakshmi, C. Ramakrishnan, G. Archunan, R. Sowdhamini, N. Srinivasan, *Int. J. Biol. Macromol.* **2014**, *63*, 119.
[2] R. K. Wierenga, E. G. Kapetaniou, R. Venkatesan, *Cell. Mol. Life Sci.* **2010**, *67*, 3961.
[3] Y. S. Kulkarni, Q. Liao, D. Petrovic, D. M. Krüger, B. Strodel, T. L. Amyes, J. P. Richard, S. Kamerlin, *J. Am. Chem. Soc.* **2017**, *139*, 10514.
[4] K. Gunasekaran, C. Ramakrishnan, P. Balaram, *J. Mol. Biol.* **1996**, *264*, 191.
[5] M. Banerjee, H. Balaram, P. Balaram, *FEBS J.* **2009**, *276*, 4169.
[6] B. Kuhlman, P. Bradley, *Nat. Rev. Mol. Cell Biol.* **2019**, *20*, 681.
[7] P. Huang, K. Feldmeier, F. Parmeggiani, D. A. Velasco, B. Höcker, D. Baker, *Nat. Chem. Biol.* **2015**, *12*, 29.
[8] M. E. Chánez-Cárdenas, D. Fernández-Velasco, E. Vázquez-Contreras, R. Coria, G. Saab-Rincón, R. Pérez-Montfort, *Arch. Biochem. Biophys.* **2002**, *399*, 117.
[9] T. V. Borchert, K. Pratt, J. P. Zeelen, M. Callens, M. E. Noble, F. R. Opperdoes, R. K. Wierenga, *Eur. J. Biochem.* **1993**, *211*, 703.
[10] J. W. Ponder, D. A. Case, *Adv. Protein Chem.* **2003**, *66*, 27.
[11] Y. Duan, C. Wu, S. Chowdhury, M. C. Lee, G. Xiong, W. Zhang, R. Yang, P. Cieplak, R. Luo, T. Lee, J. Caldwell, J. Wang, P. Kollman, *J. Comput. Chem.* **1999**, *2003*, 24.
[12] J. A. Maier, C. Martinez, K. Kasavajhala, L. Wickstrom, K. E. Hauser, C. Simmerling, *J. Chem. Theory Comput.* **2015**, *11*, 3696.
[13] G. A. Kaminski, R. A. Friesner, J. Tirado-Rives, W. L. Jorgensen, *J. Phys. Chem. B* **2001**, *105*, 6474.
[14] M. Buck, S. Bouguet-Bonnet, R. W. Pastor, A. D. MacKerell, *Biophys. J.* **2006**, *90*, L36.
[15] X. Zhai, T. L. Amyes, R. K. Wierenga, J. P. Loria, J. P. Richard, *Biochemistry* **2013**, *52*, 5928.
[16] S. C. Gill, P. H. Hippel, *Anal. Biochem.* **1989**, *182*, 319.
[17] T. C. Chang, J. H. Park, A. N. Colquhoun, C. B. Khoury, N. A. Seangmany, J. P. Schwans, *Biochem. Biophys. Res. Commun.* **2018**, *505*, 492.
[18] E. Gasteiger, A. Gattiker, C. Hoogland, I. Ivanyi, R. Appel, A. Bairoch, *Nucleic Acids Res.* **2003**, *31*, 3784.
[19] B. Plaut, J. R. Knowles, *Biochem. J.* **1972**, *129*, 311.
[20] M. K. Go, A. Koudelka, T. L. Amyes, J. P. Richard, *Biochemistry* **2010**, *49*, 5377.
[21] M. K. Go, T. L. Amyes, J. P. Richard, *J. Am. Chem. Soc.* **2010**, *132*, 13525.
[22] L. Whitmore, B. A. Wallace, *Nucleic Acids Res.* **2004**, *32*, D593.
[23] L. Whitmore, B. A. Wallace, *Biopolymers* **2008**, *89*, 392.
[24] N. Guex, M. C. Peitsch, *Electrophoresis* **1997**, *18*, 2714.
[25] H. Berendsen, D. V. Spoel, R. V. Drunen, *Comput. Phys. Commun.* **1995**, *91*, 43.
[26] M. J. Abraham, T. Murtola, R. Schulz, S. Páll, J. C. Smith, B. Hess, E. Lindahl, *SoftwareX* **2015**, *1-2*, 19.
[27] J. Lemkul, **2017**. Gromacs: MD Tutorials. http://www.mdtutorials.com/
[28] G. Bussi, D. Donadio, M. Parrinello, *J. Chem. Phys.* **2007**, *126*, 14101.
[29] M. Parrinello, A. Rahman, *J. Appl. Phys.* **1981**, *52*, 7182.
[30] MATLAB, *version 7.10.0 (R2010a)*, The MathWorks, Inc., Natick, **2010**.
[31] I. Kursula, S. Partanen, A.-M. Lambeir, D. M. Antonov, K. Augustyns, R. K. Wierenga, *Eur. J. Biochem.* **2001**, *268*, 5189.
[32] V. Olivares-Illana, H. Riveros-Rosas, N. Cabrera, M. T. Gómez-Puyou, R. Pérez-Montfort, M. Costas, A. Gómez-Puyou, *Funct. Bioinfor.* **2017**, *85*, 1190.
[33] G. Jogl, S. Rozovsky, A. E. McDermott, L. Tong, *Proc. Natl. Acad. Sci. U. S. A.* **2003**, *100*, 50.
[34] G. Alagona, C. Ghio, P. A. Kollman, *J. Am. Chem. Soc.* **1995**, *117*, 9855.
[35] M. Perakyla, T. A. Pakkanen, *Proteins* **1996**, *25*, 225.
[36] A. Lambeir, F. R. Opperdoes, R. K. Wierenga, *Eur. J. Biochem.* **1987**, *168*, 69.

SUPPORTING INFORMATION

Additional supporting information can be found online in the Supporting Information section at the end of this article.

How to cite this article: P. W. Allen, J. A. Cook, A. N. Colquhoun, E. J. Sorin, E. Tapavicza, J. P. Schwans, *Biopolymers* **2022**, e23525. https://doi.org/10.1002/bip.23525

Energetically Unfavorable Protein Angles: Exploration of a Conserved Dihedral Angle in Triosephosphate Isomerase

Patrick W. Allen, Jordan A. Cook, Anh N. Colquhoun, Eric J. Sorin, Enrico Tapavicza, Jason P. Schwans*

Department of Chemistry and Biochemistry, California State University Long Beach, Long Beach, CA, 90840, USA

*Correspondence: Jason P. Schwans, Department of Chemistry and Biochemistry, California State University Long Beach, Long Beach, CA, 90840, USA. Email: Jason.Schwans@csulb.edu

Table of Contents

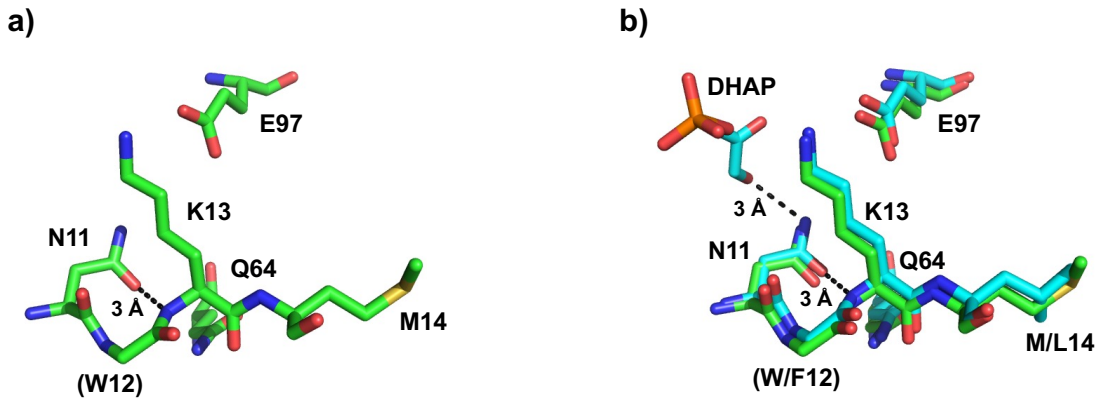

Figure S1: a) hTIM residues near K13 (PDB ID: 2JK2); b) Overlay of hTIM (PDB ID: 2JK2) and yeast (PDB ID: 1NEY) structures. hTIM is shown in green and yeast TIM in cyan. The measurements refer to distances between the N11 side chain and the K13 backbone amide and substrate (DHAP). The backbone for residue 12 is shown but the sidechain is omitted for clarity.

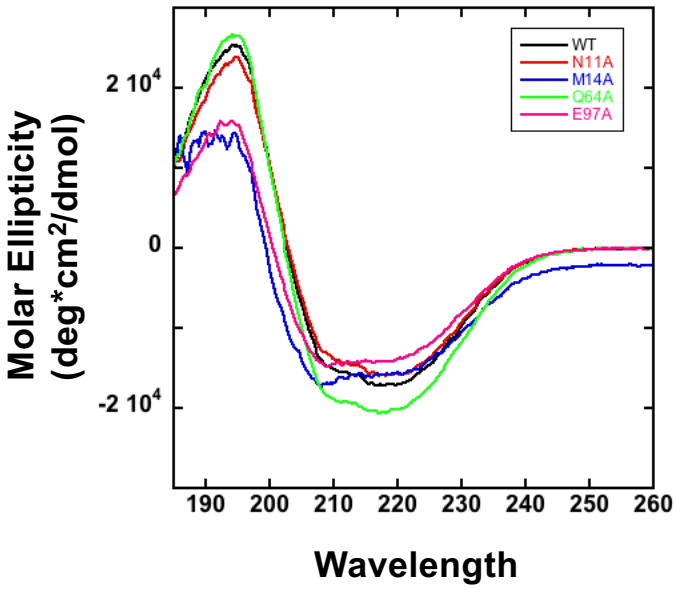

Figure S2: Circular dichroism spectra of hTIM WT, N11A, M14A, Q64A, and E97A mutants averaged from circular dichroism results. Spectra for hTIM proteins analyzed from 185 nm to 260 nm.

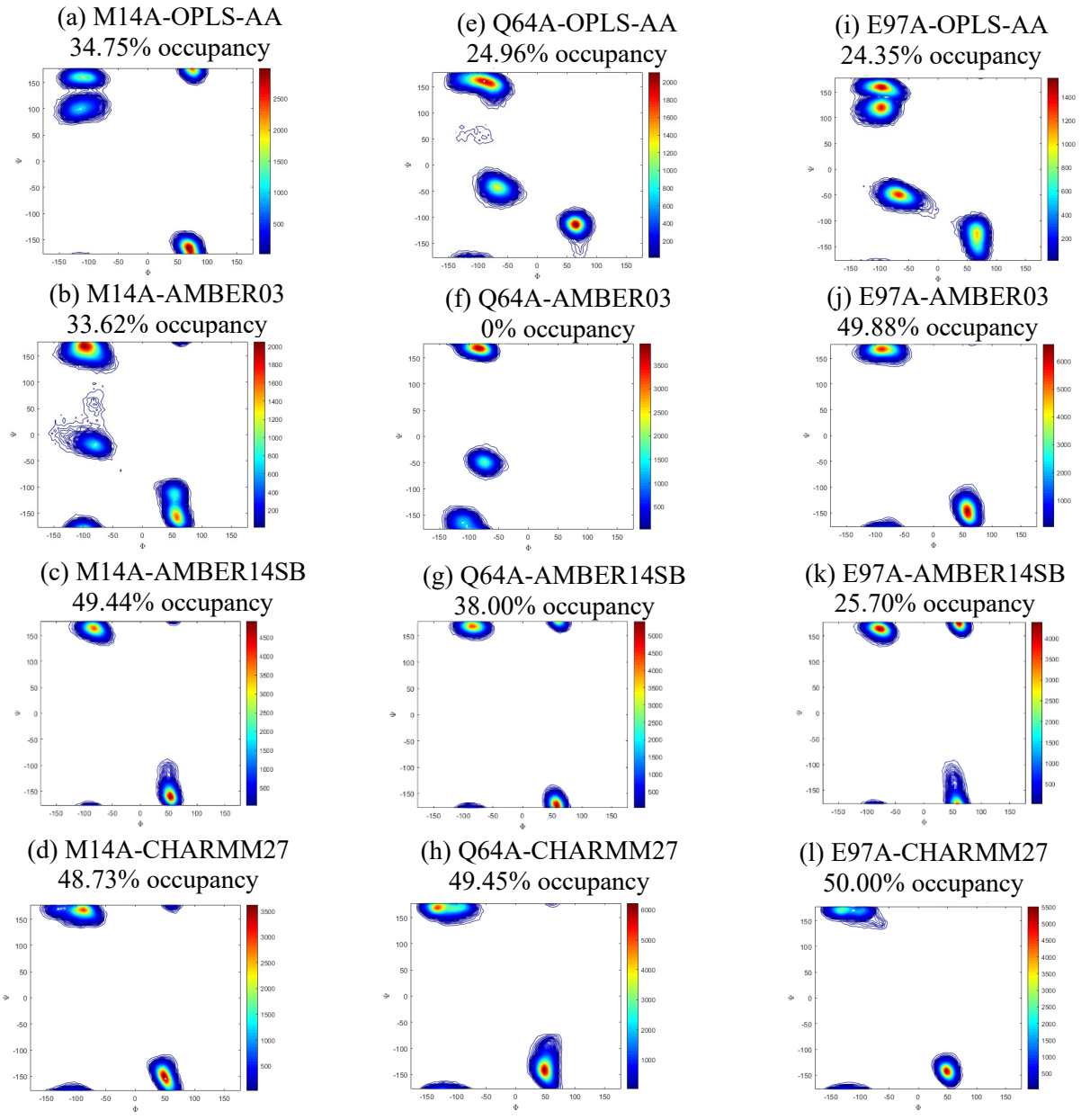

Figure S3: Heatmaps of K13 dihedral angles for M14A (a-d), Q64A (e-h), and E97A (i-l) over the final 100ns of molecular dynamics simulations with their respective K13 dihedral angle's percent occupancy of quadrant IV Ramanchandran configuration. Eachgraph represents 200,000 plotted structures plotted in Matlab.[29] The color code indicates the number of structures observed within 5^0+5^0 sized bins.

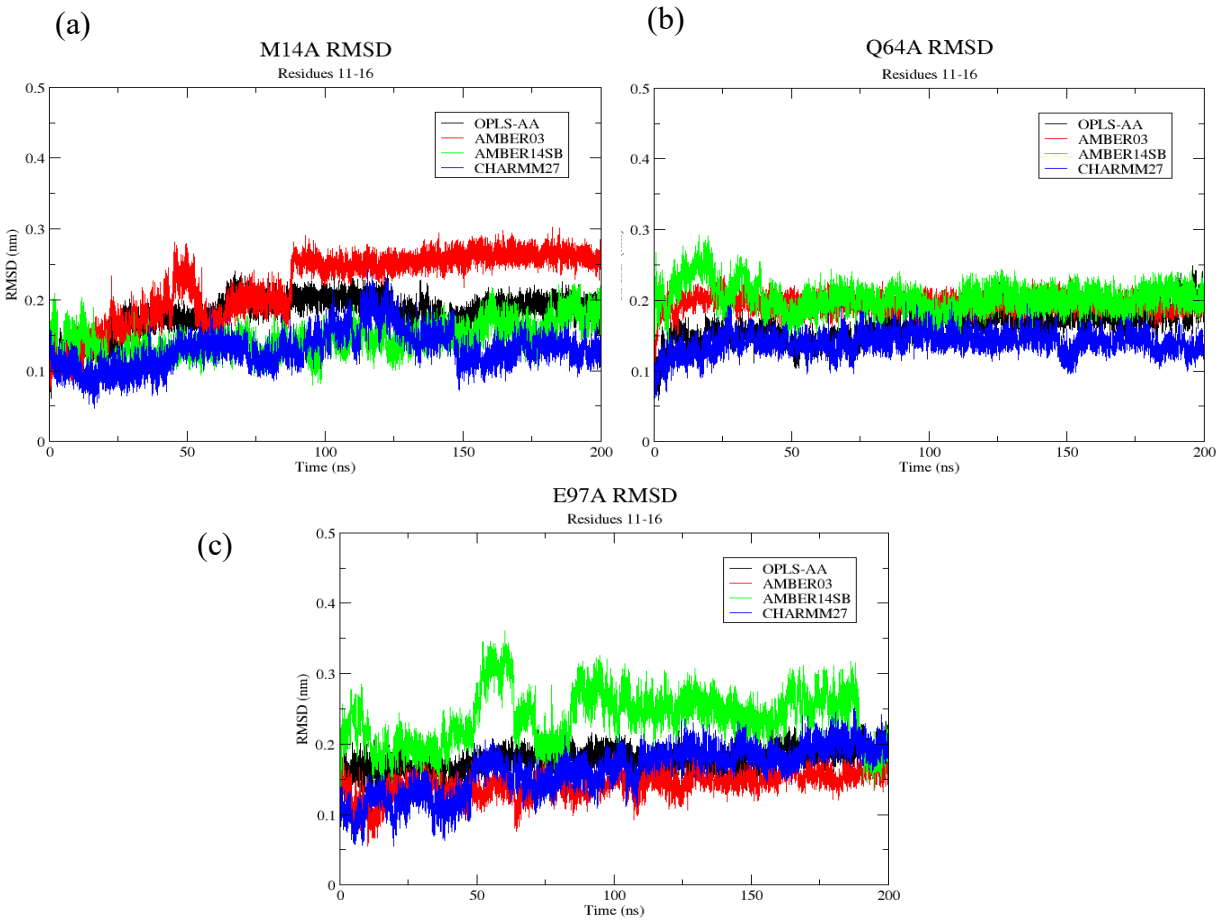

Figure S4: Root mean-square deviations of Loop 1 (residues 11-16) against whole protein for M14A (a), Q64A (b), and E97A (c). Black colored RMSD corresponds to the OPLS-AA force field, red colored RMSD to AMBER03, green colored RMSD to AMBER14SB, and blue colored RMSD to CHARMM27.